Journal of Catalysis 269 (2010) 421–431

Contents lists available at ScienceDirect

Journal of Catalysis

journal homepage: www.elsevier.com/locate/jcat

Oxidative dehydrogenation of cyclohexane over alumina-supported vanadium oxide nanoliths

H. Feng [d], J.W. Elam [b], J.A. Libera [b], M.J. Pellin [c], P.C. Stair [a,d,*]

[a] Department of Chemistry and Center for Catalysis and Surface Science, Northwestern University, Evanston, IL 60208, USA
[b] Energy Systems Division, Argonne National Laboratory, Argonne, IL 60439, USA
[c] Materials Science Division, Argonne National Laboratory, Argonne, IL 60439, USA
[d] Chemical Sciences and Engineering Division, Argonne National Laboratory, Argonne, IL 60439, USA

ARTICLE INFO

Article history:
Received 24 November 2009
Accepted 27 November 2009
Available online 28 December 2009

Keywords:
Oxidative dehydrogenation (ODH)
Cyclohexane
Vanadium oxides (VOx)
Anodic aluminum oxide (AAO)
Atomic layer deposition (ALD)

ABSTRACT

Featuring highly ordered one-dimensional nanopores, anodic aluminum oxide (AAO) makes an ideal substrate for fabrication of catalysts by atomic layer deposition (ALD). Vanadium oxide (VOx) catalysts supported on AAOs and prepared by ALD and incipient wetness impregnation are characterized by X-ray fluorescence and ultraviolet–visible (UV–Vis) spectroscopy. At low loadings (<4 V/nm^2) the supported VOx are mostly isolated monomers; polyvanadate domains are gradually formed as the surface vanadium content increases. The catalytic performance at a series of loadings (<3–32 V/nm^2), and hence different forms of VOx, for the oxidative dehydrogenation (ODH) of cyclohexane are investigated. Compared to the catalysts prepared by incipient wetness impregnation, the ALD VOx catalysts show specific activities that are between 2 and 7.5 times higher. This reflects a better dispersion of the catalytic species on the surface as synthesized by ALD. In the cyclohexane ODH reaction with the supported ALD VOx, the kinetic orders and activation energies are comparable to kinetics data reported previously for the supported VOx. The results indicate that the ALD technique can be applied as an alternative approach to synthesize the supported VOx catalysts and achieves very good dispersion even at loadings above one monolayer (8 V/nm^2). In the ODH reaction, polyvanadate sites are shown to be more active, overall, than monovanadate sites. However, numerical modeling of the reaction pathways indicates that the olefin formation rate is ~3 times faster on monomeric VOx sites than on polymeric VOx. By comparing the ODH of cyclohexane and the oxidations of cyclohexene and benzene, we find that both the sequential path and the direct path (the direct conversion from cyclohexane to benzene) are important in the oxidation process of cyclohexane.

1. Introduction

Due to its favorable thermodynamics and resistance to catalyst deactivation from coke formation, the heterogeneous oxidative dehydrogenation (ODH) of alkanes would be highly desirable for the production of olefins [1,2]. Supported vanadium oxide (VOx) catalysts have been intensively investigated for the ODH of ethane, propane, and butane because of their high activity and selectivity [2–5]. The type of support has been identified as the most important factor in determining the catalytic performance of the supported VOx [5–8]. However, the activity and selectivity for propane ODH were also shown to depend strongly on the vanadia surface coverage [3,5]. Since the molecular structure and the associated electronic and chemical properties of the supported vanadia species change progressively from isolated monomers, to two-dimensional polymers, to three-dimensional crystals with increasing surface coverage [6], the corresponding performance in propane ODH is an example of a catalytic structure-function relationship. Due to the inhomogeneity of oxide supports and the catalysts they carry, a detailed, atomic-level understanding of this relationship is still lacking. For a given surface coverage the nature of the supported vanadia species, and hence their properties, depends strongly on the method of preparation. For example, the formation of V_2O_5 crystals was observed by Raman spectroscopy at loadings of 3.6 V/nm^2 and 8 V/nm^2 in the preparation of VOx supported on γ-Al_2O_3 by impregnation using an aqueous NH_4VO_3 [9] and by the grafting of $OV(OC_3H_5)_3$ dissolved in methanol [10], respectively, due to the differences in the degree of dispersion produced by the two preparation methods. At loadings higher than one monolayer (ca. 8 V/nm^2 on alumina) characteristic peaks of crystallized V_2O_5 appear in the Raman spectra of both the

* Corresponding author. Address: Department of Chemistry and Center for Catalysis and Surface Science, Northwestern University, Evanston, IL 60208, USA. Fax: +1 847 467 1018.
E-mail address: pstair@northwestern.edu (P.C. Stair).

0021-9517/$ - see front matter © 2009 Elsevier Inc. All rights reserved.
doi:10.1016/j.jcat.2009.11.026

impregnated and the grafted VOx [11]. The formation of V_2O_5 crystals dramatically (and trivially) lowers the specific activity of the catalyst since, depending on the crystal size, a fraction of the vanadium is in the interior of the crystal and unable to participate in surface reactions [12].

In recent years atomic layer deposition (ALD) has been shown as an alternative method to synthesize supported catalysts [13–15]. In the ALD process two types of gaseous precursors are pulsed alternately, each reacting with the surface functional groups generated in the previous pulse to produce a deposition cycle. Since the surface functional groups are regenerated at the end of each deposition cycle, this technique is capable of coating as many layers of catalytic material as desired. The precise layer-by-layer deposition can effectively prevent aggregation of the catalytic species so that the catalyst has 100% dispersion on the surface. The uniformity of the catalytic materials synthesized by ALD reduces the typical inhomogeneity of heterogeneous catalysts and thereby has the potential to enhance our fundamental understanding of composition/structure/function relationships in supported heterogeneous catalysts.

The work described here makes use of a structure which provides an exceptionally uniform platform for catalytic studies that we have called the *catalytic nanolith* [16]. The nanolith is an array of uniform, straight channels with controllable dimensions in the range 10–100 nm. It can be coated with catalytic layers and sealed in a flow reactor so that the reactants must pass through the catalytic pores during reaction, and all the pores have the same dimensions. An extremely uniform coating throughout the entire length of the nanolith channels can be realized by the ALD technique [17]. Thus, each channel has identical catalytic layers. Moreover, there is no change in surface area due to pore blocking and negligible change in pore diameter even at high catalyst loadings unlike some previous studies [18]. Therefore, surfaces with well-dispersed catalytic species, at loadings up to one monolayer, and no pore blockage are made possible by the combination of the nanolith and the ALD technique. Initial studies also indicate that the nanolith structure minimizes the contribution of homogeneous, radical reactions under ODH conditions and produces a higher activity and selectivity to olefin than a comparable catalyst in the form of a powder [16]. Finally, the nanolith structures used in the present study are only 70 μm thick, making it possible to perform UV–Vis absorption measurements in transmission rather than in diffuse reflectance.

The reaction studied here is the oxidative dehydrogenation of cyclohexane. In contrast to ethane, propane, and butane, ODH of cyclohexane has received much less attention. Lopez and coworkers studied the performance of different groups of catalysts for this reaction, including silica and niobia supported vanadia, V, Fe, and Ce phosphates, and protonic and transition metal exchanged ZSM-5 zeolites, finding that the major product of this reaction is either benzene or COx (CO and CO_2) [19]. Usually benzene is not considered to be a useful product in this reaction since the hydrogenation of benzene is an industrial process for cyclohexane production. The valuable product from this reaction is cyclohexene, which is an intermediate in the production of adipic acid, the monomer for Nylon 6, 6 [20]. A traditional way to produce cyclohexene is by the dehydration of cyclohexanol, which is obtained from the oxidation of cyclohexane in liquid phase [21]. A direct conversion from cyclohexane to cyclohexene through a heterogeneously catalyzed process is highly desirable but no catalytic system has shown a meaningful yield of cyclohexene. From a fundamental point of view the study of cyclohexane ODH provides more information about the catalytic reaction pathways than with comparable studies using propane. With propane the formation of COx is the inevitable result of breaking three or more C–H bonds. This is not the case for cyclohexane where benzene is formed by breaking one C–H bond on each methylene group. Consequently, a catalyst that is very active only for breaking C–H bonds will favor benzene formation, while the same catalyst will only make COx from propane. COx formation from cyclohexane requires breaking of multiple C–H bonds on a single methylene, C–C scission, O-insertion, or a radical process. The ability to form two different hydrocarbon products in this reaction also makes it possible to evaluate the contributions from a reaction path where the formation of benzene occurs during a single adsorption of the cyclohexane reactant on the catalyst compared to a true sequential reaction path that involves cyclohexene as the intermediate. These issues will be discussed further in terms of a structure–function relationship.

2. Experimental

The nanolith supports were prepared using the method previously described [16]. A two-step anodization of high purity aluminum disks (Alfa Aesar, 99.99%) was carried out in 0.3 M oxalic acid (Fisher 99.9%) at a constant potential of 40 V, resulting in 40 nm pores with an average pore to pore separation of 110 nm [22,23]. The thickness (pore length) of the nanolith, ~70 μm in this case, is determined by the duration of the second-step anodization. The aluminum disks were masked during fabrication to preserve an aluminum border around the perimeter of the nanolith. This enabled the nanoliths to be sealed in the reactor using commercial compression fittings. Before any catalyst was loaded, the nanolith pores were coated with 1 nm of Al_2O_3 to completely cover electrolyte impurities incorporated into the oxide material during anodization. Detailed descriptions about the introduction of coatings in nanoliths can be found elsewhere [17]. In brief, alumina ALD was carried out at 200 °C in a viscous flow reactor [24]. Ultra high purity nitrogen (Airgas, 99.999%) was used as the purge gas. The layer-by-layer growth of alumina was achieved by alternately exposing the substrates to trimethyl aluminum (Aldrich, 97%) and water for 8-cycles using a quasi-static reactor operation mode in which the reactor is pumped down to 0.1 Torr after each dose and purge.

The VO_x catalysts were introduced onto the nanoliths by both wet impregnation and ALD. For wet impregnation an aqueous solution of NH_4VO_3 (Aldrich, 99.99%) was dropped onto one side of the nanolith and at the same time a slight vacuum was applied from the other side to draw the solution through the pores and to assist the evaporation of liquid. To ensure a complete wetting of the pore walls by the liquid, a dilute solution (3.2×10^{-3} mol/l) was used so that the volume of the solution was much greater than that of the nanolith pores. The precursor solution was applied from both sides of the nanolith alternately, and the application and drying procedure was repeated several times until the desired amount of vanadium was introduced. The samples were first dried at 150 °C for 1 h and then calcined in oxygen at 500 °C for 5 h.

Using the ALD procedure, VOx was deposited in an integral number of sub-monolayer cycles using vanadium oxytriisopropoxide (Aldrich, 99.98%)/(hydrogen peroxide + water) as the precursors. A dose-purge-dose-purge timing sequence of 45–30–45–30 s was used in each cycle to deposit layer(s) of VOx onto the nanolith at 100 °C, 1.1 Torr, with a nitrogen flow rate of 240 sccm/min [16]. Different numbers of cycles (1–18) of VOx were deposited to make samples with a series of loadings. After coating the catalytic materials, the samples were tested in the catalysis experiments without further treatment. After initial catalysis testing, the ALD samples were calcined in oxygen at 500 °C for 2 h and then re-tested under the same conditions to probe for reproducibility and catalyst aging.

X-ray Fluorescence Spectroscopy (XRF) was used as a non-destructive method to characterize the amount of vanadium supported in the nanolith. The spectra were measured with an Oxford ED2000 instrument. The XRF data were calibrated by the results from inductively coupled plasma (ICP) measurements taken with a Varian Vista-MPX instrument. To prepare the samples for ICP, the nanoliths were removed from the aluminum mounting ring and dissolved in 10% phosphoric acid solution. The primary atomic emission wavelength of vanadium at 292.4 nm was used for analysis.

UV–Vis spectra of the catalysts were measured with a Cary 500 UV–Vis-NIR spectrometer under ambient conditions. Since the nanoliths are transparent, the spectra were measured in transmission using a double beam configuration with a blank nanolith as the reference. For each nanolith sample, UV–Vis spectra were recorded both before and after catalysis testing and after subsequent calcinations.

The catalytic experiments were carried out in a flow reactor with the nanolith sealed in a modified Swagelok VCR fitting [16]. Prior to performing the catalytic experiments, the reactor was coated with 50 nm of Al_2O_3 by ALD to reduce interference from reactions catalyzed by the metal reactor itself. The nanolith seal was carefully tightened to a force where the upstream gas pressure was stable and no leak was detected. Quartz chips (14–30 mesh) were used to fill the empty space in the reactor and minimize possible gas phase reactions [2]. Cyclohexane vapor was introduced into the reaction system using a helium gas bubbler. Oxygen (Airgas, 99.99%) was used as the oxidant, and a mixture of methane and helium (Matheson, 1.00:99.00) was used as the balance gas. With the exception of experiments designed to determine reaction orders, cyclohexane ODH reactions were performed with cyclohexane:oxygen:balance gas compositions of 1:2:97 and 1:8:91. Reaction gas mixtures of 1:8:91 were employed for comparing the ODH of cyclohexane, cyclohexene, and benzene to ensure a low conversion (<10%) of oxygen and consequently to eliminate the possible influence of oxygen concentration on reaction rates. Catalytic reactions were carried out in the temperature range 400–480 °C with a reactant flow rate of 10 sccm/min at atmospheric pressure. Reaction products were analyzed by a HP 6890 gas chromatograph equipped with flame ionization (FID) and thermal conductivity (TCD) detectors for probing the organic and inorganic products, respectively. Methane was used as an internal standard to convert signals between the two detectors. The measured conversion of methane was zero under the conditions of the catalysis experiments. The published values of the response factors for the FID and TCD were used to correct the peak areas obtained from the two detectors [25]. In our reports the selectivity is defined as the percentage of the reactant that is converted to a specific product:

$$\text{Selectivity(Product)} = \frac{\text{Moles of Reactant to Form Product}}{\text{Moles of Reactant Consumed}}$$

A Hitachi S4700 scanning electron microscope (SEM) was used to study the surface topology and structure of the nanoliths. The aluminum oxide material was removed from the aluminum sealing ring for thermal gravimetric analysis (TGA). TGA was performed using a Q50 TGA instrument. During the measurement the temperature was increased from room temperature up to 1000 °C at a rate of 20 °C/min in a nitrogen atmosphere.

3. Results and discussion

3.1. Nanolith-supported VOx

A typical nanolith consists of 10^{11} straight pores. Each pore is 40 nm in diameter and 70 μm long. The total surface area of the nanolith, measured from both the pore geometry and by BET, is ~0.05 m^2 [16]. The base material that forms the nanolith structure, prior to ALD, is an amorphous alumina with impurity electrolyte anions, such as oxalates and sulfates, incorporated into the alumina framework during the anodization process [26]. TGA measurements show that the decomposition temperatures of these incorporated impurities are as high as 890–950 °C. Since these temperatures exceed the melting point of the supporting aluminum ring, calcination is not a feasible way to remove the impurities. To avoid the possible interference from these impurities in the catalytic reactions, the nanoliths are coated with 1 nm of pure Al_2O_3 by ALD to completely cover the incorporated anions. In blank catalytic tests without VOx the ALD alumina-coated nanoliths exhibited low, stable background reaction rates (0.1–0.5% conversion from 400 °C to 480 °C). The diameter of the pores is reduced from 40 nm to 38 nm by the ALD alumina coating. The corresponding reduction in the total surface area is ~5%.

The aqueous impregnation of vanadium containing precursors and subsequent calcination can form a two-dimensional monolayer structure of supported VOx on the surface of alumina, titania, and niobia [3,4]. The monolayer loading of VOx depends on the type of support. On γ-alumina, this loading is reported to be 13 μmol/m^2 or approximately 8 V/nm^2 [3]. On the surface of Si (0 0 1), the structure of the coated ALD alumina has been shown to be amorphous [27]. Since the surface of amorphous alumina is structurally similar to γ-alumina [28], the value of 8 V/nm^2 is adopted as the monolayer loading when introducing VOx onto the nanolith by wet impregnation.

The amount of VOx loaded by ALD was first measured by the non-destructive XRF technique. An accurate calibration of the XRF signals using known standards was not available since it was not possible to fabricate a series of homogeneous powder support samples that had the same composition as the nanolith and a known amount of VOx. Instead, ICP measurements of the nanolith samples were used to provide a calibration for the XRF data. In obtaining the XRF results, the vanadium surface concentrations were calculated based on the measured amount of the VOx species, and the total weight and surface area of the nanolith. The calculated vanadium surface concentrations are listed in Table 1.

The quantity of vanadium coated by each cycle of ALD is much less than the monolayer loading (8 V/nm^2), which means that a single cycle of VOx ALD does not completely cover the surface. This is likely due to steric constraints imposed by the rather bulky ligands on the vanadia precursor. The amount of vanadium loaded by ALD does not increase linearly for the first few ALD cycles. In Table 1 the XRF/ICP results show that the increase in vanadium for the first few ALD cycles was larger than that for the subsequent cycles. Since in the ALD of VOx the vanadium precursor attachment is a self-limiting process determined by the available surface functional (hydroxyl) groups, the change in vanadium loading with each cycle may indicate a gradual decrease in the density of surface hydroxyls as more cycles of VOx are coated [29].

Table 1
The vanadium surface density and UV–Vis edge energies of wet impregnated (W.I.) and ALD VOx measured by XRF and ICP.

VOx sample	Surface density (V/nm^2)	E_g (eV)
W.I. 1 L	8	3.69
W.I. 2 L	16	3.52
W.I. 4 L	32	3.37
ALD 1-cycle	2.8	3.64
ALD 2-cycles	3.7	3.48
ALD 4-cycles	6.2	3.33
ALD 8-cycles	9.0	3.17
ALD 12-cycles	11.7	3.11
ALD 18-cycles	14.1	3.04

An intense, broad absorption band is typically observed in UV–Vis spectra of the supported VOx catalysts due to oxygen to tetrahedral V^{5+} charge transfer [30,31]. The absorption edge energy (E_g) can be used to determine the state of the VOx species since it is related to the number of V–O–V bonds or the domain size of vanadia polymers on the surface [32,33]. Fig. 1 shows the transmission UV–Vis spectra of the nanoliths loaded by ALD and wet impregnation. The spectra measured before and after catalytic reaction and subsequent calcination are essentially identical. In these spectra the peaks at ~225 nm (5.52 eV) and ~275 nm (4.51 eV) are assigned to the isolated monomeric tetrahedral vanadium species [34,35]. In the UV–Vis spectra of the ALD samples, a peak at ~315 nm (3.94 eV) becomes pronounced at loadings $\geqslant$6.2 V/nm^2 (4-cycle ALD VOx), indicating the presence of oligomeric distorted tetrahedral VOx [36,37]. The edge energies, E_g, were determined from the *x*-intercept of the linearized near edge region of absorption vs. $h\nu$, i.e. using the method of Tandon and Gupta [38]. E_g values from the wet impregnated and ALD-loaded samples are listed in Table 1.

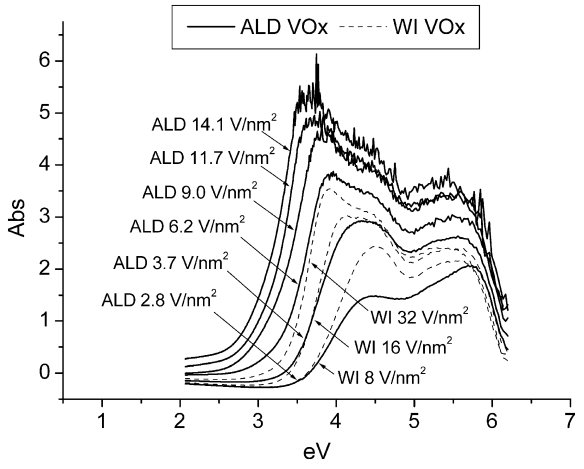

Fig. 1. The UV–Vis absorption spectra of ALD-synthesized and the wet impregnated VOx supported on the catalytic nanolith.

The UV–Vis absorption edge from both the ALD and wet impregnated VOx samples exhibits a red shift as the loading increases. Gao and Wachs reported an approximately linear correlation between the edge energy and the number of V–O–V covalent bonds around the central V^{5+} cations based on the measurements of standard compounds [32]. The edge energy values of the standard compounds with 0–5 V–O–V bonds range between 3.48 and 2.35 eV. Their results are plotted in Fig. 2 and are used as the reference for comparing with the measured edge energies of VOx supported on the nanolith.

The edge energy of 1-cycle ALD VOx sample is 3.64 eV, which corresponds to an isolated, tetrahedrally coordinated VO_4 species according to the E_g values in the reference compounds. This result for the first cycle of ALD VOx is consistent with the expected chemistry between surface hydroxyl groups (Al–OH) and the isopropoxide ligands where only V–O–Al bonds are formed in the first part of the cycle. Removal of the remaining isopropoxide ligands by hydrogen peroxide/water in the second part of the cycle is expected to produce V–OH species (see Scheme 1). As more cycles of VOx are deposited, V–O–V bonds will be formed in a reaction between the V–OH groups and the vanadyl precursor, resulting in a gradual increase in the average VOx domain size and a corresponding decrease in the edge energy. The lowest edge energy is obtained on the nanolith with the highest VOx loading. However, even at the highest loading (18-cycles of VOx), the E_g value (3.04 eV) is still much higher than that of the V_2O_5 crystal, indicating that at this loading the ALD VOx has fewer V–O–V bonds than V_2O_5; a two-dimensional structure is still the predominant form of VOx on the surface.

Interestingly, despite the large difference in VOx loadings between the impregnated and the ALD VOx samples, the edge energies of the 1-cycle, 2-cycle, and 4-cycle ALD samples appear to be close to their 1-layer, 2-layer, and 4-layer wet impregnated counterparts, indicating that the predominant forms of the VOx sites are nearly the same for these pairs of ALD and impregnated samples. These results reflect the different qualities of the two types of catalyst loading methods. The ALD technique enables an extremely uniform dispersion of species on the surface [39]. In contrast, incipient wetness impregnation and the following calcinations cannot guarantee complete spreading of the catalytic

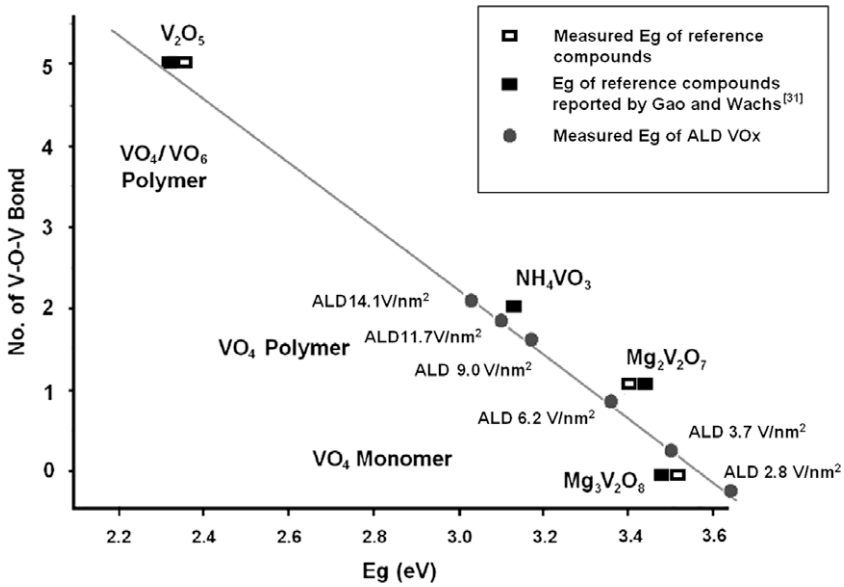

Fig. 2. Number of V–O–V bonds plotted against the edge energies of vanadium oxide reference compounds and the ALD-synthesized, nanolith-supported VOx edge energy positions with correlated V–O–V bond numbers. The solid line represents the correlation between the number of V–O–V bonds and the edge energies of the reference compounds reported by Gao and Wachs [31].

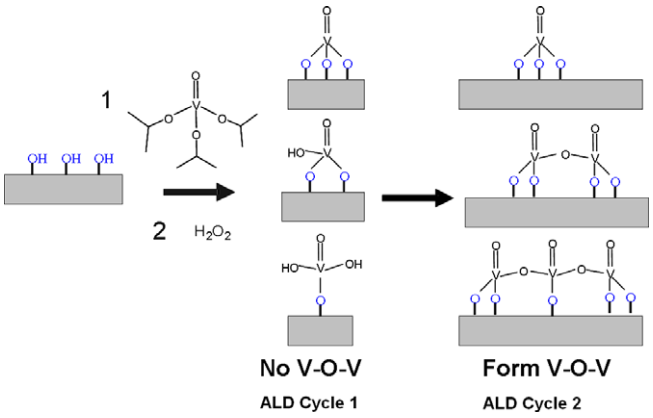

Scheme 1. Possible molecular structures of surface vanadyl species formed by atomic layer deposition of vanadyl triisopropoxide.

species; particles of V_2O_5 may form even at loadings significantly below a theoretical monolayer [11]. Consequently, a relatively smaller vanadium density is expected on some areas of the surface. This effect appears to be exacerbated during impregnation of the nanoliths, as evidenced by an observed accumulation of the precursor solution near the boundary of the AAO and the aluminum ring so that the layers of crystalline V_2O_5 are very likely to be formed in these regions. The UV–Vis absorption measurements probe only the central portion (~30%) of the AAO material where the vanadium surface density is likely to be lowest. The results of reaction studies reported below suggest that the central portion of the nanolith primarily determines the catalytic performance.

3.2. Catalytic properties of VOx supported on alumina nanoliths

3.2.1. Comparison between the ALD VOx and wet impregnated VOx

In all the catalysis tests the absolute conversions measured for duplicate samples prepared with the same composition vary less than 5%. The catalytic layers appear to be stable under our calcination and reaction conditions. Fresh samples, tested immediately after the ALD VOx loading, and those re-tested after calcination in oxygen show little difference in catalytic performance.

Fig. 3a and b depict the catalytic conversion and selectivity results for ALD (1–4 cycles) and wet impregnated (1–4 layers) VOx at 450 °C, respectively. The catalysis data are plotted against the absorption edge energies in the UV–Vis spectra. The conversion/selectivity performance is similar for each pair of W.I. and ALD samples having comparable absorption edge energies. Since the catalytic performance (especially the selectivity) is dependent on the structure of the VOx species, the similarities in the catalytic performance provide additional support for the statement made earlier that the structures of the catalytic sites are essentially the same for the pairs of ALD and W.I. samples with comparable edge energies.

To quantitatively compare the specific activities or turnover frequencies (TOF's) between samples, knowledge of the number of active vanadium oxide sites is required. A number of methods for counting redox-active sites have been proposed in the literature. Prominent among these are methods that make use of methanol chemisorption and reaction [40–44], but it has not been established that methanol is necessarily a suitable probe molecule for counting the active sites in alkane ODH reactions. More recently a method based on the anaerobic oxidation of ethanol has been reported that could be generalized to count sites for the ODH of cyclohexane [45]; however, due to the low loading of vanadia in the nanoliths and the multitude of products formed, the application of this method in cyclohexane ODH is technically very difficult and currently beyond our capabilities.

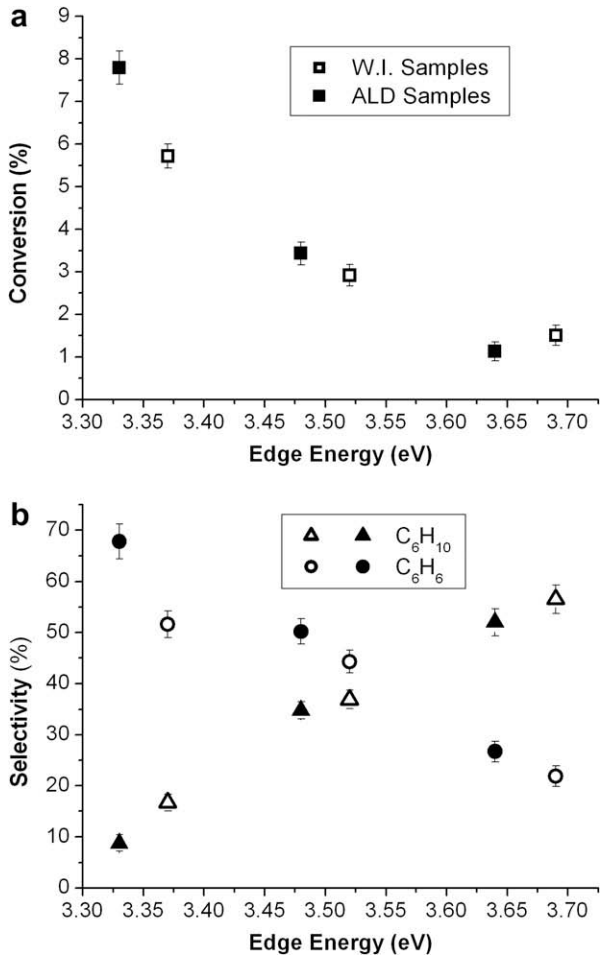

Fig. 3. Conversion (a) and selectivity (b) vs. absorption edge energy for ALD-synthesized (solid symbols) and wet impregnated (hollow symbols) catalysts at 450 °C.

For the present discussion an "effective TOF" is calculated by normalizing the measured rates by the total vanadium content determined by XRF/ICP. As we shall see, the effective TOF and the selectivities observed for ALD- and W.I.-prepared catalysts are sensitive to the nature of the catalytic species. Since the ALD technique produces uniformly dispersed surface VOx species, it is anticipated that all vanadium atoms contribute to the activity at loadings $\leqslant 9$ V/nm^2 and that the effective TOF and the "true" TOF are approximately equal. For the W.I. samples the UV–Vis data suggest that the vanadia species are poorly dispersed.

The effective TOF's are compared as Arrhenius plots of ln(TOF) vs. $1/T$ in Fig. 4. Effective TOF's for the wet impregnated samples are substantially lower than the ALD samples due to poor dispersion. The percentage of active VOx species on the wet impregnated nanoliths can be estimated by comparing with the TOF of the ALD samples that have similar vanadia surface species (by UV–Vis) using:

$$\text{Active VOx } \% = \frac{\text{TOF}_{\text{W.I.}}}{\text{TOF}_{\text{ALD}}} \times 100\% \quad (1)$$

Using Eq. (1) we find that 45 ± 1% of the VOx is active on the nanolith at the one monolayer wet impregnation loading; this percentage drops to 21 ± 2% and 13 ± 1% as the loading increases to 2-layers and 4-layers by impregnation. These percentages are similar

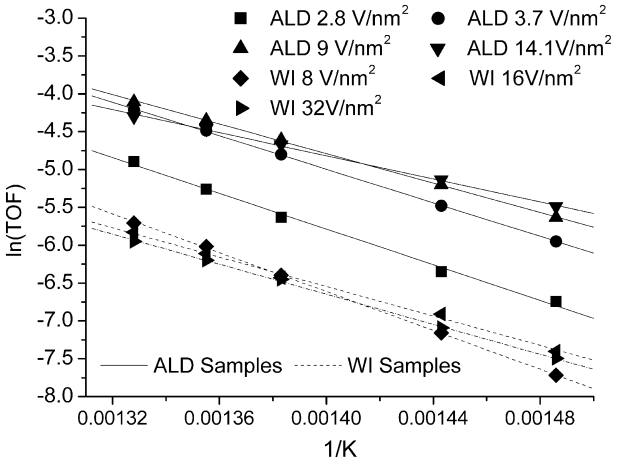

Fig. 4. Plots of log(TOF) vs. 1/T for ALD-synthesized and wet impregnated vanadium oxide catalysts.

to the values reported in reference [45] for ethanol oxidation by vanadia supported on γ-alumina also prepared by wet impregnation.

The reaction activation energies can be obtained from the slopes of the plots in Fig. 4. The activation energies range from 107 to 81 kJ/mol for 1–4 layers of wet impregnated VOx and from 98 to 63 kJ/mol for the 1–18 cycles of ALD VOx (see Table 2). The activation energies measured in our system are consistent with those reported by Lopez and coworkers in studies of the same reaction (60–100 kJ/mol depending on the substrates) [19]. Therefore, neither the AAO scaffold nor the ALD loading technique seems to impart unusual chemical properties in the supported VOx other than enhanced specific activity. This implies that the ALD technique can be used as an alternative method to synthesize conventional supported catalysts. Further discussion of the VOx catalytic properties in the ODH of cyclohexane focuses on the ALD samples.

3.3. Activity analysis

The observed rate of a heterogeneous catalytic reaction can be influenced by the surface kinetics, pore diffusion resistance, and film mass transfer. In the nanolith catalytic system where the reactants are forced through the nanopores, diffusion resistance will not significantly affect the reaction rate. Conversions are low (less than 10%) in most experiments, so that mass transfer and product concentrations will not significantly influence reaction rates. Our previous analysis of the dependence of conversion on flow rate in the nanolith catalytic system showed that the reaction is first-order in cyclohexane [16]. The reaction order with respect to cyclohexane and oxygen was also measured by varying the concentration of one reactant while holding that of the other constant. The measured cyclohexane reaction rate increases linearly with cyclohexane concentration, consistent with the flow rate experiments, and remains almost constant at all oxygen concentrations (unless the O_2 partial pressure is very close to 0). Fig. 5 presents a log–log plot of reaction rate vs. cyclohexane and oxygen concentrations measured at 450 °C. The reaction orders determined from the slopes of these plots are 0.9 ± 0.1 for cyclohexane and 0.1 ± 0.1 for oxygen. The uncertainties are due to variations in the measured rates. This shows that the ODH reaction is essentially first-order in cyclohexane and zero order in oxygen. This result is consistent with the reported reaction orders in the ODH of propane and butane over the supported VOx [46–48]. The resultant rate equation signifies a typical Mars–van Krevelen redox mechanism, in which lattice oxygen in the catalytic site is responsible for the dehydrogenation process, and gas phase oxygen only serves as a reservoir of the oxidant that continuously replenishes lattice oxygen on the surface.

The TOF of cyclohexane measured using the ALD catalysts (see Fig. 6) exhibits some interesting trends. The TOF increases dramatically as the loading increases from 2.8 to 6.2 V/nm^2 or from 1 to 4 cycles of VOx ALD. It is relatively constant between 6.2 and 11.7 V/nm^2 (4–12 cycles of VOx ALD) and finally decreases at higher loading. Normally at loadings higher than one monolayer a continuous decline in the TOF is expected since part of the vanadia will be buried and will be unable to participate in the reaction. At loadings lower than 11.7 V/nm^2 (1–12 cycles of VOx ALD), the VOx species are in a highly dispersed form so that nearly all vanadia species are available for catalysis. The initial increase in TOF with loading reflects changes in the intrinsic catalytic activity of the vanadia sites. From Table 2 we see that the activation energy decreases as the VOx loading increases. This trend indicates that the surface VOx species formed at higher loadings are more active for the ODH of cyclohexane.

Analysis of the UV–Vis spectra shows that the VOx species formed by 1-cycle of ALD are isolated monomers, consistent with Scheme 1. The V–O–V bond connecting two adjacent V centers begins to form and gradually prevails on the surface as more cycles of VOx are deposited. Apparently the presence of these V–O–V bonds makes two major changes to the catalyst: first, they replace V–O–Al bonds so that the related chemical properties, such as the

Table 2
The activation energies of wet impregnated and ALD VOx supported on the nanoliths.

Sample	E_a (kJ/mol)
W.I. 1-layer	106.6
W.I. 2-layer	80.6
W.I. 4-layer	82.4
ALD 1-cycle	98.1
ALD 2-cycle	92.1
ALD 4-cycle	83.5
ALD 8-cycle	80.3
ALD 12-cycle	65.8
ALD 18-cycle	63.3

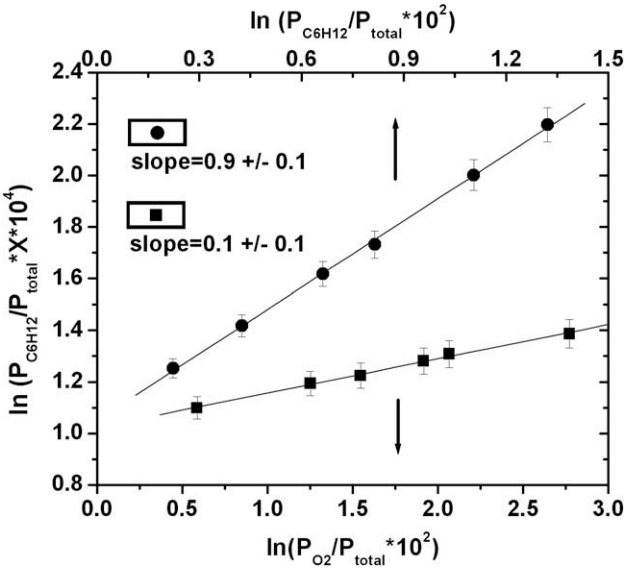

Fig. 5. The logarithm of cyclohexane reaction rate vs. the logarithm of cyclohexane and oxygen concentrations measured using the ALD-synthesized catalyst with a vanadium loading of 3.7 V/nm^2. The reaction rate is first-order (0.9 ± 0.1) in cyclohexane and approximately zero order (0.1 ± 0.1) in oxygen.

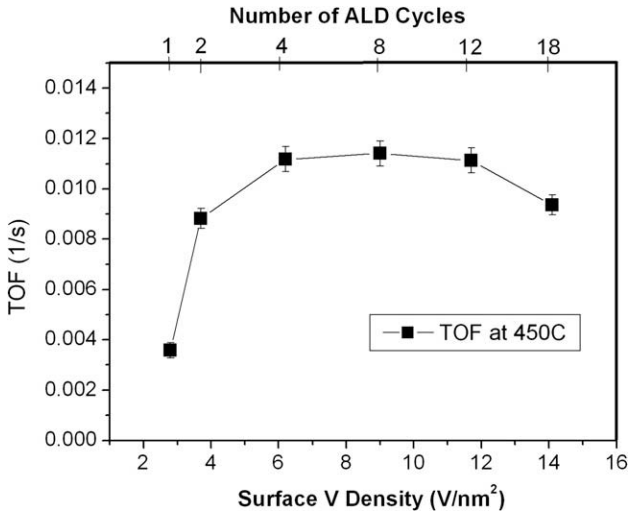

Fig. 6. The turnover frequency vs. Vanadium loading for ALD-synthesized catalysts at 450 °C.

reducibility of the vanadia, are enhanced; second, the adjacent V centers are brought closer and consequently a concerted reaction mechanism that involves the attendance of more than one V center becomes possible. The increased TOF at high VOx loadings is due to one or both of these effects.

The dependence of turnover frequency on the domain size of VOx is not unique to the cyclohexane ODH reaction. A similar correlation has been found by Iglesia and coworkers for the ODH of propane [49]. They attribute the change in TOF to changes in the reducibility of the VOx species. Since oxidative dehydrogenation of the hydrocarbon involves the reduction–oxidation of the V^{5+} center, the ease of reduction of the catalytic site will largely determine the activity of the catalyst. Therefore, polyvanadate domains, which are more easily reduced by hydrogen than vanadate monomers, are more active in the ODH reactions. Because the ODH of cyclohexane and propane share many common features, especially the hydrocarbon activation step, a common explanation for the dependence of activity on loading is expected.

The fact that the V centers on the surface are brought closer at higher loadings may also be a factor in their increased catalytic activity. The proximity of V centers will enable the formation of multiply bonded reaction intermediates, which are more strongly adsorbed to the catalytic sites and consequently less likely to desorb from the surface before reaction. If the adsorption of cyclohexane onto the catalytic site is due to interaction between a C atom and a V center, the spatial distance between adjacent V centers will largely determine whether the formation of multiply bonded species is possible. With the V–O–V bonding geometry, the shortest distance between two V centers is approximately 0.32 nm, based on crystallographic data of di-vanadium compounds [50]. By comparison, the average distance between two isolated V centers sitting next to each other is ~0.58 nm at an average surface density of 3 V/nm^2 (which corresponds to the surface vanadium density of a 1-cycle ALD sample). The C–C bond length in the cyclohexane molecule is 0.154 nm, therefore the distances between C–C atoms in the 1,2, 1,3, and 1, 4 positions are 0.15, 0.24, and 0.29 nm, respectively. The estimated V–C bond length is approximately 0.14 nm based on the reported ionic radius of V^{5+} (0.072 nm) and the covalent radius of C (0.07 nm) [51]. Using these estimates a cyclohexane molecule can bond to the two vanadium centers in a V–O–V bond via 1,2, 1,3, or 1,4 diadsorbed intermediates while this is impossible with the two isolated V centers. Multiply bonded intermediates will facilitate the dehydrogenation process and possibly affect the reaction path by promoting multiple C–H bond breaking on the same catalytic site. This would lead to direct conversion from cyclohexane to benzene. As we see below, a kinetic analysis of reaction pathways indicates that such a direct conversion is favored at monolayer vanadium surface density (~9.0 V/nm^2).

In contrast to the results presented here, Tian and Wachs reported that for the ODH of propane the specific activity of surface monomeric and polymeric vanadia species is the same but depends strongly on the nature of the support cations, analogous to a ligand effect [33]. While, it would seem that such a ligand effect should also apply to the formation of V–O–V bonds, it may be that the ODH of cyclohexane is more sensitive to vanadia species structure because of its larger size and the possibility of multiple bonds to the vanadia. The presence of polymeric vanadia clearly plays an important role in the direct reaction path from cyclohexane to benzene, which accounts for a large portion of the cyclohexane conversion. In the case of propane, a comparable direct reaction path does not exist since the only deep oxidation products are COx, which requires C–O insertion or C–C breaking in addition to C–H bond activation.

3.4. Analysis of selectivity

The conversion and product selectivities for the reaction run at 450 °C over the series of VOx catalysts are illustrated by the data in Fig. 7. Consistent with the low reaction order in oxygen partial pressure shown in Fig. 5, the results from experiments using cyclohexane:oxygen mixtures of 1:2 and 1:8 are identical. As the conversion increases with vanadium loading, the selectivities to CO and CO_2 increase slightly with values that are very similar to what has been reported for the ODH of propane catalyzed by vanadia supported on γ-alumina [9] and explained by sequential oxidation reactions that typically accompany increases in conversion in the range of low conversion. The selectivities to cyclohexene and benzene change much more dramatically. Cyclohexene is the most abundant product (55%) at a vanadium density of 2.8 V/nm^2 but much less abundant (10%) at 6.2 V/nm^2. In contrast the selectivity to benzene increases from 26% to 68%. The formation of cyclohexene and benzene is due to the breaking of multiple C–H bonds but no more than one on each methylene group. In contrast COx formation involves fundamentally different reactions such as C–C bond breaking, oxygen insertion, or the breaking of both C–H

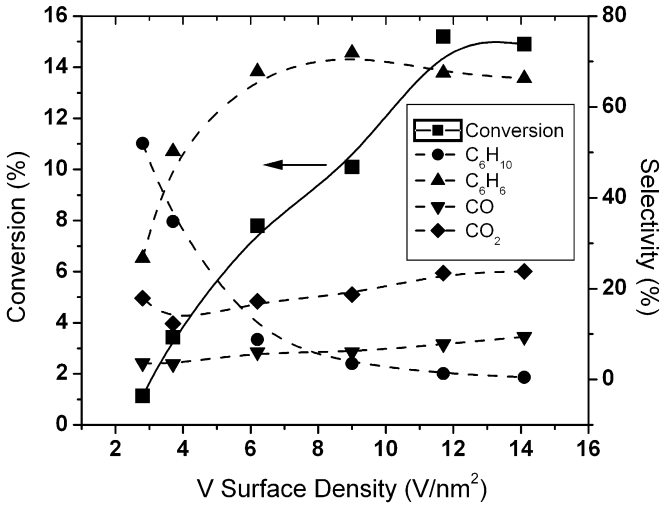

Fig. 7. Conversion and selectivity vs. vanadium loading for ALD-synthesized catalysts at 450 °C. The lines are not fits but intended to make the trends clearer.

bonds on a methylene group. We argue below that the pronounced change in selectivities toward cyclohexene and benzene is due to a variation in the kinetics of competing reaction pathways with increasing vanadia loading.

In the ODH of alkanes, the conversion is of primary importance in determining the selectivity because the partial oxidation product is typically easier to oxidize than the reactant so that the selectivity drops significantly with increasing conversion. To evaluate the intrinsic selectivity of different catalyst materials, the preferred method is to compare experiments at constant reaction temperature and conversion by adjusting the space velocity. This is not feasible for the catalytic nanoliths because the amount of catalyst in the reactor is fixed by the nanolith and the range of flow rates is limited by the mechanical stability of the nanolith material. The conversion can be adjusted by changing the reaction temperature, and for this reaction it appears that the temperature and space velocity have a very similar influence on the selectivity/yield to cyclohexene in the tested temperature range. Fig. 8 displays the C_6H_{10} yield vs. C_6H_{12} conversion curves of the ALD samples with vanadium densities of 2.8 and 9.0 V/nm^2 measured at different reaction temperatures (and a fixed space velocity) or at different space velocities (and a fixed temperature). For each sample the curves measured at different temperatures or at different space velocities overlap very well. This is also true for the yields of benzene, CO and CO_2. Furthermore, it is clear that the yield of cyclohexene is much higher on the sample with a low VOx loading than with a high VOx loading. Taken together the results depicted in Figs. 7 and 8 point to a strong dependence of selectivity on the nature of the vanadia species that is distinct from the differences in conversion.

The selectivity in cyclohexane ODH is determined by the relative importance of the reaction pathways shown in Scheme 2. The selectivity to cyclohexene and benzene is determined by the relative rates of converting cyclohexane to these two products (k_1 and k_2), and the rate of the further oxidation of cyclohexene (k_3). The conversion from cyclohexane to benzene via the formation and further oxidation of cyclohexene (the $k_1 \rightarrow k_3$ route) is a sequential reaction path while the direct conversion from cyclohexane to benzene (k_2) is considered an independent direct reaction. Both the sequential path and the direct path likely share a partially dehydrogenated cyclohexane as a common reaction intermediate, in a structure that resembles an adsorbed olefin. This intermediate can either desorb from the surface to produce cyclohexene (the k_1 route), or lose another C–H bond and head for benzene (the k_2 route). A change in the catalyst that increases the ratio

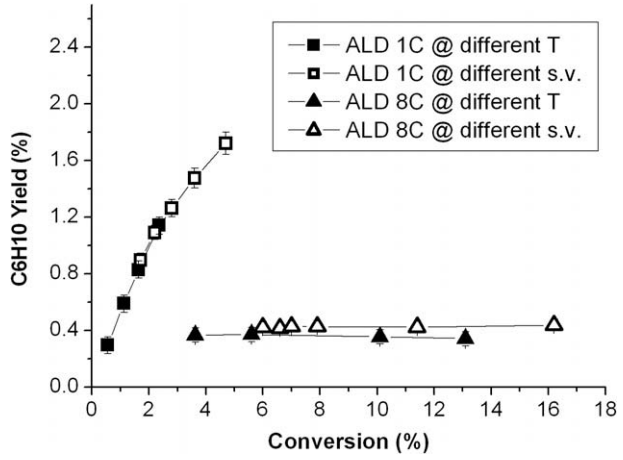

Fig. 8. The C_6H_{10} yield vs. C_6H_{12} conversion curves of the 1-cycle and 8-cycle ALD VOx samples measured at different temperatures or at different space velocities.

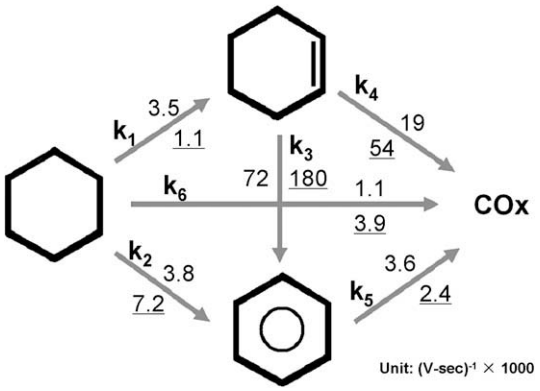

Scheme 2. Cyclohexane ODH reaction pathways. The numbers represent the rate coefficients of the different reaction paths at 450 °C of the two samples with 3.7 and 9.0 V/nm^2. The numbers with underscore represent the rate coefficients of the sample with 9.0 V/nm^2.

of rates k_2/k_1 will lead to more benzene through the direct reaction route. In the sequential reaction route, increasing the rate of cyclohexene dehydrogenation (k_3) will lower the selectivity to the olefin and consequently raise the selectivity to benzene. COx can be formed by the oxidation of benzene (the k_5 route), cyclohexene (the k_4 route), or even directly from cyclohexane (the k_6 route).

To study the roles of the sequential reaction route and the direct routes in the ODH of cyclohexane as a function of temperature and their relationship to the nature of the VOx catalyst, oxidation reactions using cyclohexane, cyclohexene, and benzene as reactants were studied on catalysts with VOx loadings of 3.7 and 9.0 V/nm^2. The different reactants were studied using the same reaction conditions (the same hydrocarbon space velocity, temperature range and an oxygen/hydrocarbon ratio of ~8/1 to ensure a very low oxygen conversion and thus pseudo-first-order conditions for all the ODH reactions).

Comparing the conversion/selectivity patterns of cyclohexene and benzene as reactants to those of cyclohexane, we can conclude that the direct conversion from cyclohexane to benzene (the k_2 route in Scheme 2) plays a significant role in benzene formation from cyclohexane. For example, at 400 °C where the benzene conversion to COx is very low, the yield of benzene from cyclohexane ODH is determined by the sum of the consecutive ($k_1 \rightarrow k_3$) and direct (k_2) routes. Assuming that the percent conversion of cyclohexene is the same regardless of whether it is fed as a reactant or produced by cyclohexane ODH (equivalent to pseudo-first-order kinetics, differential reaction conditions, and a well-mixed reactor), the yield of benzene from the consecutive route ($Y_{1\rightarrow3}(benzene)$) can be estimated by Equation (2) and compared to the *measured* yield of benzene from cyclohexane ODH:

$$Y_{1\rightarrow3}(benzene) = Y_3(benzene) \times \frac{Y_1(cyclohexene)}{Y_{3+4}(cyclohexene)} \quad (2)$$

where $Y_3(benzene)$ is the yield of benzene via the direct reaction (reaction 3), $Y_1(cyclohexene)$ is the yield of cyclohexene from cyclohexane ODH (reactions 1), and $Y_{3+4}(cyclohexene)$ is the percentage of cyclohexene remaining when cyclohexene is fed as a reactant. Fig. 9 presents the product selectivity patterns in cyclohexane ODH at 400 °C for the catalysts with VOx loadings of 3.7 and 9.0 V/nm^2. The hatched area represents the contribution from the consecutive path estimated from Eq. (2). For both catalysts the olefin formation and reaction rates cannot account for the observed yields of benzene. In fact, the direct reaction appears to be the dominant route to benzene. Moreover, the branching between consecutive and direct routes appears to change significantly with the structure of the catalyst. As shown in Fig. 9, a much larger portion

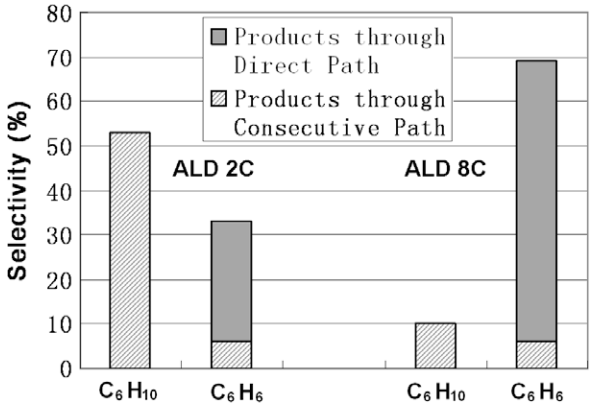

Fig. 9. The product distribution patterns of the ALD catalysts with VOx loadings of 3.7 and 9.0 V/nm^2 in the ODH of cyclohexane at 400 °C. The hatched areas in the charts represent the contributions from the consecutive paths.

of benzene is produced from the direct path on the catalyst with a V loading of 9.0 V/nm^2.

To provide a more quantitative comparison of sequential and direct reaction paths and the role of other reactions, a first-order kinetic analysis of Scheme 2 was performed, analogous to that of reference [52]. This simple analysis ignores the effects of inhibition by any of the intermediates and products. Fig. 5 confirms that cyclohexane ODH is nearly first-order for cyclohexane and zero order for oxygen. The product selectivities were the same for cyclohexane:oxygen ratios of 1:2 and 1:8, consistent with near zero order oxygen dependence in the reactions of cyclohexene and benzene. Indeed, the ODH of propene and butene were reported to follow the Mars–van Krevelen mechanism and were first-order in olefin and low order in oxygen [47]. Thus, the assumption of first-order kinetics should be adequate at the low conversions employed here.

Since gas flow in the nanolith pores conforms to the mixed flow regime (diffusion + plug flow) [16], the nanolith system is similar to a continuous-feed, batch reactor. Thus, the conversion of cyclohexane is given by:

$$-\frac{d[C_6H_{12}]}{dt} = k_1[C_6H_{12}] + k_2[C_6H_{12}] + k_6[C_6H_{12}] \quad (3)$$

Corresponding equations are applied to describe the conversions of cyclohexene and benzene:

$$-\frac{d[C_6H_{10}]}{dt} = -k_1[C_6H_{12}] + k_3[C_6H_{10}] + k_4[C_6H_{10}] \quad (4)$$

$$-\frac{d[C_6H_6]}{dt} = -k_2[C_6H_{12}] - k_3[C_6H_{10}] + k_5[C_6H_6] \quad (5)$$

The pseudo-first-order rate coefficients are written as $k_i = A_i \exp\left(\frac{E_i}{RT}\right)$ The coupled differential equations are solved numerically, and the rate coefficient parameters are obtained from experiments with benzene, cyclohexene, and cyclohexane as the reactants by least squares fitting the product yields [53]. The rate coefficient parameters for reaction 5 in Scheme 2 (A_5 and E_5) are first determined from the experiment with reactant benzene, in which the benzene consumption is expressed as:

$$-\frac{d[C_6H_6]}{dt} = k_5[C_6H_6] \quad (6)$$

The resulting rate coefficient parameters are used in the determination of the parameters for reactions 3 and 4 (A_3, E_3, and A_4, E_4) from the experiment with reactant cyclohexene, where

$$-\frac{d[C_6H_{10}]}{dt} = k_3[C_6H_{10}] + k_4[C_6H_{10}] \quad (7)$$

$$-\frac{d[C_6H_6]}{dt} = -k_3[C_6H_{10}] + k_5[C_6H_6] \quad (8)$$

Finally, the parameters for reactions 1, 2, and 6 are determined from the experiment with reactant cyclohexane. Altogether there are 12 parameters obtained from fitting 30, independent, data points. The solid curves obtained from the model are compared to the experimental results in Fig. 10. The fits between the experiments and

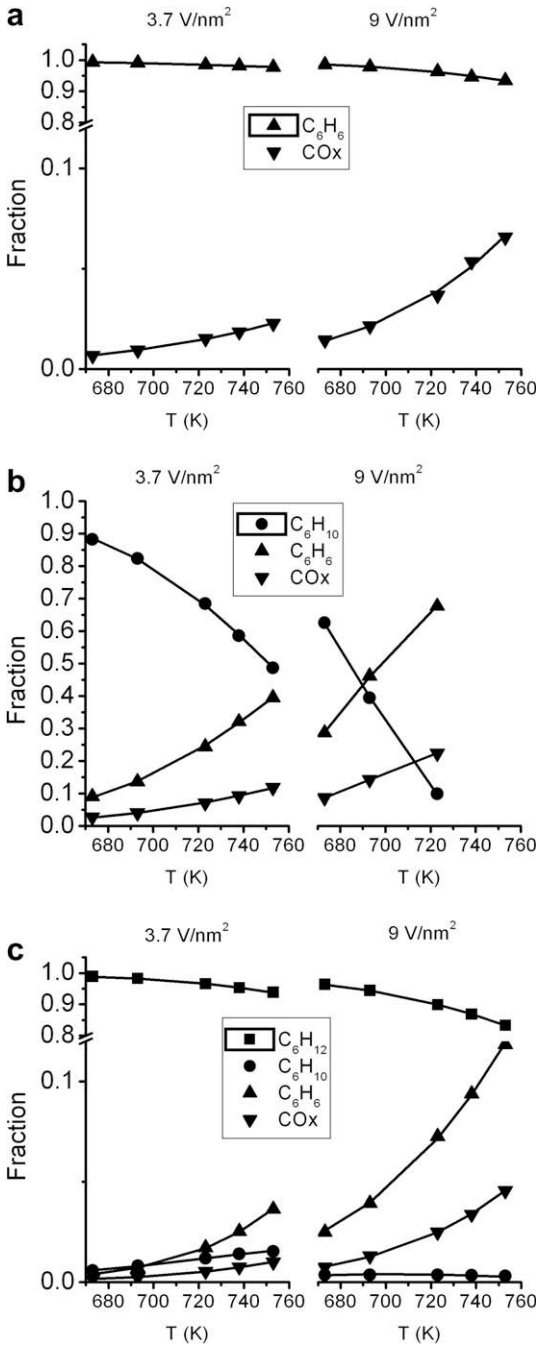

Fig. 10. Comparison of experimental and fitted yields vs. temperature using the ALD-synthesized catalyst with vanadium loadings of 3.7 and 9.0 V/nm^2 for reactant benzene (a), cyclohexene (b), and cyclohexane (c). For the reaction of cyclohexene with the higher loading sample only the three data points at lower temperatures are used in the modeling because at higher reaction temperatures the conversion of cyclohexene is 100%.

the model are very good for both catalysts. Correlation coefficients are all above 0.99, and the largest percent standard deviation for the calculated k_i's is 5% with typical values nearer to 1%.

What is of interest here is how the partitioning along reaction paths changes between high and low loading of vanadia. This can be seen by examining the values of the rate coefficients given in Table 3 relative to k_1 for the low loading catalyst. We see that on the sample with the low catalyst loading (3.7 V/nm^2), a large fraction (56–48%) of the reacted cyclohexane follows the sequential reaction path and a smaller fraction (33–38%) is directly converted to benzene at the lower reaction temperatures; at higher temperatures more cyclohexane (45–51%) is directly converted to benzene through the k_2 route. The k_2/k_1 ratio ranges between 0.6 and 1.3 depending on the reaction temperature. On the high loading sample (9.0 V/nm^2), at all reaction temperatures, nearly 70% of the reacted cyclohexane is directly converted to benzene through the direct path and in this case the k_2/k_1 ratio is 5.2–6.8. These trends show that the form or structure of the catalytic site is a major factor determining the reaction path in the ODH of cyclohexane. As discussed above, during the cyclohexane activation process, the multi-adsorbed intermediate can be formed on polyvanadate domains containing the V–O–V bond, suggesting that this configuration facilitates the direct conversion from cyclohexane to benzene. Additionally, the larger VOx polymeric domains possess more lattice oxygen and are more easily reduced; therefore they are more likely to be capable of multiple C–H breaking steps on the same catalytic site as required for the direct reaction mechanism.

Scheme 2 presents the rate coefficients of the different reaction paths at 450 °C from the two samples. Comparing these rate coefficients, it is interesting to note that although the overall reaction rate of the sample with 9.0 V/nm^2 is higher than the lower loading sample, the latter has a higher rate of cyclohexene formation (k_1) in accordance with the yields shown in Fig. 8. The same trend can also be observed at all other temperatures. This suggests that cyclohexene is formed mainly (if not exclusively) on monomeric vanadyl centers. It is possible that at some point the conversion from cyclohexane to cyclohexene and to benzene share a common reaction intermediate, which then desorbs from the monomer sites to form cyclohexene but undergoes further C–H breaking to form benzene on polymeric sites.

These results demonstrate that the primary route to nonselective products from cyclohexane is via breaking of multiple C–H bonds to form benzene and ultimately carbon oxides. The modeling also shows that the most important pathway at high loadings of vanadium oxide is not the sequential reaction of a primary cyclohexene product but the direct surface reaction (the k_2 reaction path in Scheme 2). It is likely that the same process applies to the formation of carbon oxides in the ODH of other alkanes, such as propane, by supported vanadium oxide, and that this is controlled, in part, by the structure of the vanadium oxide species.

Table 3
Rate coefficients for the reaction paths shown in Scheme 2.

T (°C)	400	420	450	465	480
(a) The rate coefficients of different reactions routes (shown in Scheme 2) obtained from the simulation on the 2-cycle ALD VOx sample. The units are (V-s)$^{-1}$ × 1000					
k_1	1.5	2.1	3.5	4.4	5.4
k_2	0.9	1.7	3.8	5.4	7.8
k_3	22	36	72	99	133
k_4	6.5	10	19	27	37
k_5	1.7	2.3	3.6	4.5	5.6
k_6	0.3	0.6	1.1	1.5	2.1
(b) The rate coefficients of different reactions routes (shown in Scheme 2) obtained from the simulation on the 8-cycle ALD VOx sample. The units are (V-s)$^{-1}$ × 1000					
k_1	0.5	0.6	1.1	1.4	1.8
k_2	2.6	3.9	7.2	9.5	12
k_3	36	70	180	285	420
k_4	10	21	54	82	126
k_5	1.4	2.1	3.9	5.3	6.9
k_6	0.8	1.2	2.4	3.2	4.2

4. Conclusions

VOx catalysts of different structures were synthesized on the surface of catalytic nanoliths either by performing cycles of ALD using vanadium oxytriisopropoxide /hydrogen peroxide + water as the precursors or by incipient wetness impregnation. XRF/ICP measurements indicate that each ALD cycle enables sub-monolayer loading (1/3 of a monolayer) of VOx onto the surface. In the UV–Vis spectra of the nanolith-supported catalysts, the absorption edge energies reveal that the predominant form of the supported VOx transforms from monovanadate sites to polyvanadate domains as the loading increases from ~3 to 14 V/nm^2.

The nanoliths loaded with the ALD VOx show ~2 to 5 times higher specific activities than those with the impregnated VOx, which reflects the better dispersion of the catalytic species synthesized by ALD. The activation energies of the ALD and impregnated VOx were in the range 60–100 kJ/mol; these values are comparable to those reported in the literature. These results imply that the chemical properties of the supported VOx are not altered by the nanolith scaffold or the ALD loading technique. Therefore ALD can be applied as an alternative method to prepare supported catalysts.

The cyclohexane ODH reaction over ALD VOx is found to be approximately first-order in hydrocarbon and zero order in oxygen. The observed reaction orders are in agreement with the Mars–Van Krevelen redox mechanism, which is typical for the ODH of alkanes over supported metal oxide catalysts. In the ODH reaction of cyclohexane, a rise in the catalytic activity (TOF) together with a decrease in the activation energy is observed with the increasing loading of the catalyst, implying that the polyvanadate domains are more active than the monovanadate sites. However, the selectivity to cyclohexene drops dramatically as the VOx loading increases. Even when compared at the same conversions, the samples with higher VOx loadings always show lower selectivity to cyclohexene. The reaction network for cyclohexane ODH is analyzed by numerical simulation of the oxidation of cyclohexane, cyclohexene, and benzene under the same experimental conditions. It is found that both sequential and direct paths exist in the cyclohexane oxidation process. The formation of the deep oxidation products, benzene and COx, can proceed through either the sequential path or the direct paths, depending on the structure of the supported catalysts. When the catalyst loading is low (3.7 V/nm^2), 56–36%, depending on the temperature, of the reacted cyclohexane follows the sequential reaction path and 33–51% is directly converted to benzene. At high loading (9.0 V/nm^2), regardless of the reaction temperature, over 70% of the reacted cyclohexane is directly converted to benzene through the direct path. Although the overall reaction rate of the sample with 9.0 V/nm^2 is much higher than that of the lower loading sample, the lower loading sample has a higher (~3 times) rate of cyclohexene formation. This suggests that cyclohexene is formed mainly on monomeric vanadyl centers.

Acknowledgment

This work was supported by the US Department of Energy, Office of Basic Energy Science, under Contracts DE-AC02-06CH11357 and DE-FG02-03-ER15457.

References

[1] E.A. Mamedov, V. Cortes Corberan, Appl. Catal. A 127 (1995) 1–40.
[2] H.H. Kung, Adv. Catal. 40 (1994) 1–38.
[3] A. Khodakov, B. Olthof, A.T. Bell, E. Iglesia, J. Catal. 181 (1999) 205–216.
[4] L.E. Briand, O.P. Tkachenko, M. Guraya, X. Gao, I.E. Wachs, W. Gruenert, J. Phys. Chem. B 108 (2004) 4823–4830.
[5] I.E. Wachs, B.M. Weckhuysen, Appl. Catal. A 157 (1997) 67–90.
[6] N. Ballarini, F. Cavani, A. Cericola, C. Cortelli, M. Ferrari, F. Trifiro, G. Capannelli, A. Comite, R. Catani, U. Cornaro, Catal. Today 91–92 (2004) 99–104.
[7] G. Deo, I.E. Wachs, J. Catal. 146 (1994) 323–334.
[8] A.A. Lemonidou, L. Nalbandian, I.A. Vasalos, Catal. Today 61 (2000) 333–341.
[9] M.D. Argyle, K.D. Chen, A.T. Bell, E. Iglesia, J. Catal. 208 (2002) 139–149.
[10] M.A. Vuurman, I.E. Wachs, J. Phys. Chem. 96 (1992) 5008–5016.
[11] G.T. Went, S.T. Oyama, A.T. Bell, J. Phys. Chem. 94 (1990) 4240–4246.
[12] F. Cavani, N. Ballarini, A. Cericola, Catal. Today 127 (2007) 113–131.
[13] J. Keranen, A. Auroux, S. Ek, L. Niinisto, Appl. Catal. A: General 228 (2002) 213–225.
[14] J. Keranen, C. Guimon, E. Iiskola, A. Auroux, L. Niinisto, Catal. Today 78 (2003) 149–157.
[15] R.J. Silvennoinen, O.J.T. Jylha, M. Lindblad, H. Osterholm, A.O.I. Krause, Catal. Lett. 114 (2007) 135–144.
[16] H. Feng, J.W. Elam, J.A. Libera, M.J. Pellin, P.C. Stair, Chem. Eng. Sci. 64 (2009) 560–567.
[17] P.C. Stair, C. Marshall, G. Xiong, H. Feng, M.J. Pellin, J.W. Elam, L. Curtiss, L. Iton, H. Kung, M. Kung, H.-H. Wang, Top. Catal. 39 (2006) 181–186.
[18] E.V. Kondratenko, M. Baerns, Appl. Catal. A 222 (2001) 133–143.
[19] M. Panizza, C. Resini, G. Busca, E. Fernandez Lopez, V. Sanchez Escribano, Catal. Lett. 89 (2003) 199–205.
[20] K. Sato, M. Aoki, R. Noyori, Science (Washington DC) 281 (1998) 1646–1647.
[21] W. Yao, Y. Chen, L. Min, H. Fang, Z. Yan, H. Wang, J. Wang, J. Mol. Catal. A: Chem. 246 (2006) 162–166.
[22] T. Gao, G. Meng, J. Zhang, S. Sun, L. Zhang, Appl. Phys. A: Mater. Sci. Process. 74 (2002) 403–406.
[23] H. Masuda, K. Fukuda, Science 268 (1995) 1466–1468.
[24] J.W. Elam, M.D. Groner, S.M. George, Rev. Sci. Instrum. 73 (2002) 2981–2987.
[25] W.A. Dietz, J. Gas Chromatogr. 5 (1967) 68–71.
[26] G. Xiong, J.W. Elam, H. Feng, C.Y. Han, H.-H. Wang, L.E. Iton, L.A. Curtiss, M.J. Pellin, M. Kung, H. Kung, P.C. Stair, J. Phys. Chem. B 109 (2005) 14059–14063.
[27] R. Katamreddy, R. Inman, G. Jursich, A. Soulet, C. Takoudis, J. Electrochem. Soc. 153 (2006) C701–C706.
[28] G. Gutierrez, B. Johansson, Phys. Rev. B 65 (2002) 104202–104211.
[29] J.C. Badot, S. Ribes, E.B. Yousfi, V. Vivier, J.P. Pereira-Ramos, N. Baffier, D. Lincot, Electrochem. Solid-State Lett. 3 (2000) 485–488.
[30] B.M. Weckhuysen, D.E. Keller, Catal. Today 78 (2003) 25–46.
[31] G. Centi, S. Perathoner, F. Trifiro, A. Aboukais, C.F. Aissi, M. Guelton, J. Phys. Chem. 96 (1992) 2617–2629.
[32] X. Gao, I.E. Wachs, J. Phys. Chem. B 104 (2000) 1261–1268.
[33] H. Tian, I. Ross Elizabeth, E. Wachs Israel, J. Phys. Chem. B 110 (2006) 9593–9600.
[34] P. Knotek, L. Capek, R. Bulanek, J. Adam, Top. Catal. 45 (2007) 51–55.
[35] P. Van Der Voort, M.G. White, M.B. Mitchell, A.A. Verberckmoes, E.F. Vansant, Spectrochim. Acta Part A 53A (1997) 2181–2187.
[36] M.L. Pena, A. Dejoz, V. Fornes, F. Rey, M.I. Vazquez, J.M. Lopez Nieto, Appl. Catal. A 209 (2001) 155–164.
[37] M. Baltes, K. Cassiers, P. Van Der Voort, B.M. Weckhuysen, R.A. Schoonheydt, E.F. Vansant, J. Catal. 197 (2001) 160–171.
[38] S.P. Tandon, J.P. Gupta, Phys. Status Solidi 38 (1970) 363–367.
[39] J.W. Elam, G. Xiong, C.Y. Han, H.H. Wang, J.P. Birrell, U. Welp, J.N. Hryn, M.J. Pellin, T.F. Baumann, J.F. Poco, J.H. Satcher Jr., J. Nanomater. (2006) 1–5.
[40] I.E. Wachs, T. Kim, E.I. Ross, Catal. Today 116 (2006) 162–168.
[41] I.E. Wachs, J.-M. Jehng, W. Ueda, J. Phys. Chem. B 109 (2005) 2275–2284.
[42] L.J. Burcham, L.E. Briand, I.E. Wachs, Langmuir 17 (2001) 6164–6174.
[43] L.J. Burcham, L.E. Briand, I.E. Wachs, Langmuir 17 (2001) 6175–6184.
[44] M. Badlani, I.E. Wachs, Catal. Lett. 75 (2001) 137–149.
[45] H. Nair, C.D. Baertsch, J. Catal. 258 (2008) 1–4.
[46] K. Chen, A.T. Bell, E. Iglesia, J. Phys. Chem. B 104 (2000) 1292–1299.
[47] A. Dejoz, J.M. Lopez Nieto, F. Melo, I. Vazquez, Ind. Eng. Chem. Res. 36 (1997) 2588–2596.
[48] K. Inumaru, M. Misono, T. Okuhara, Appl. Catal. A: General 149 (1997) 133–149.
[49] K. Chen, A. Khodakov, J. Yang, A.T. Bell, E. Iglesia, J. Catal. 186 (1999) 325–333.
[50] R. Gopal, C. Calvo, Acta Crystallogr. Sect. B 30B (1974) 2491–2493.
[51] R.D. Shannon, Acta Crystallogr. Sect. A A32 (1976) 751–767.
[52] S.T. Oyama, A.M. Middlebrook, G.A. Somorjai, J. Phys. Chem. 94 (1990) 5029–5033.
[53] Scientist by Micromath Inc.